

Synthesis and in Vivo Evaluation of [ $^{123}\text{I}$ ]Melanin-Targeted Agents

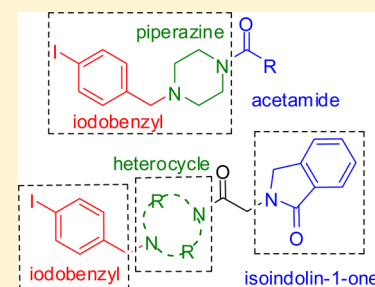
Maxine P. Roberts,<sup>†,§</sup> Vu Nguyen,<sup>†,§</sup> Mark E. Ashford,<sup>†</sup> Paula Berghofer,<sup>†</sup> Naomi A. Wyatt,<sup>†</sup>  
Anwen M. Krause-Heuer,<sup>†,||</sup> Tien Q. Pham,<sup>†</sup> Stephen R. Taylor,<sup>†,⊥</sup> Leena Hogan,<sup>†</sup> Cathy D. Jiang,<sup>†</sup>  
Benjamin H. Fraser,<sup>†</sup> Nigel A. Lengkeek,<sup>†</sup> Lidia Matesic,<sup>†</sup> Marie-Claude Gregoire,<sup>†</sup> Delphine Denoyer,<sup>‡,#</sup>  
Rodney J. Hicks,<sup>‡</sup> Andrew Katsifis,<sup>†,∇</sup> and Ivan Greguric<sup>\*,†</sup>

<sup>†</sup>LifeSciences Division, Australian Nuclear Science and Technology Organisation (ANSTO), Locked Bag 2001, Kirrawee DC, New South Wales 2232, Australia

<sup>‡</sup>Centre for Molecular Imaging, Peter MacCallum Cancer Centre, 12 St. Andrew's Place, East Melbourne, Victoria 3002, Australia

## S Supporting Information

**ABSTRACT:** This study reports the synthesis, [ $^{123}\text{I}$ ]radiolabeling, and biological profile of a new series of iodinated compounds for potential translation to the corresponding [ $^{131}\text{I}$ ]radiolabeled compounds for radionuclide therapy of melanoma. Radiolabeling was achieved via standard electrophilic iododestannylation in 60–90% radiochemical yield. Preliminary SPECT imaging demonstrated high and distinct tumor uptake of all compounds, as well as high tumor-to-background ratios compared to the literature compound [ $^{123}\text{I}$ ]4 (ICF01012). The most favorable compounds ([ $^{123}\text{I}$ ]20, [ $^{123}\text{I}$ ]23, [ $^{123}\text{I}$ ]41, and [ $^{123}\text{I}$ ]53) were selected for further biological investigation. Biodistribution studies indicated that all four compounds bound to melanin containing tissue with low in vivo deiodination; [ $^{123}\text{I}$ ]20 and [ $^{123}\text{I}$ ]53 in particular displayed high and prolonged tumor uptake (13% ID/g at 48 h). [ $^{123}\text{I}$ ]53 had the most favorable overall profile of the cumulative uptake over time of radiosensitive organs. Metabolite analysis of the four radiotracers found [ $^{123}\text{I}$ ]41 and [ $^{123}\text{I}$ ]53 to be the most favorable, displaying high and prolonged amounts of intact tracer in melanin containing tissues, suggesting melanin specific binding. Results herein suggest that compound [ $^{123}\text{I}$ ]53 displays favorable in vivo pharmacokinetics and stability and hence is an ideal candidate to proceed with further preclinical [ $^{131}\text{I}$ ] therapeutic evaluation.



## INTRODUCTION

Melanoma is an aggressive form of skin cancer with metastatic tendencies and is currently the fourth most commonly diagnosed cancer in Australia (excluding basal and squamous cell carcinoma of the skin), following breast cancer in women or prostate cancer in men and bowel and lung cancer.<sup>1,2</sup> Despite the increasing incidence of this disease, surgical excision with margins based on Breslow thickness and anatomical location still remains the most effective treatment of melanoma grades 1–3. Treatment by surgical resection is limited once the melanoma has metastasized to secondary locations (grade 4).<sup>3</sup> Grade 4 melanotic tumors that exhibit excessive melanin pigmentation presents an attractive target for both diagnostic and therapeutic applications.<sup>4–6</sup>

Of the iodine radioisotopes, iodine-123 ( $^{123}\text{I}$ ) has the most favorable properties for SPECT imaging purposes with a short half-life (13.2 h), low patient radiation exposure and provides the possibility of complementary radiolabeling of the same compound with other isotopes, such as iodine-131 ( $^{131}\text{I}$ ).<sup>7,8</sup> Iodine-131 is not an ideal isotope for imaging but is the most commonly used radionuclide for therapy due to its relatively long half-life (8.0 days) and emission of  $\beta$ -particles that penetrate a few millimeters in tissue, making it useful for treatment of solid tumors.<sup>6,9,10</sup> Hence, [ $^{123}\text{I}$ ] and [ $^{131}\text{I}$ ] can be used as complementary isotopes for initial broad biological

evaluation, followed by targeted radiopharmaceuticals for treatment of malignant melanoma.

A number of methods have been investigated for selective delivery of various diagnostic and therapeutic radionuclides to malignant melanoma; of these, numerous [ $^{123}\text{I}$ ] labeled benzamide derivatives have demonstrated high uptake in melanotic tissue.<sup>7–12</sup> Studies of the first [ $^{123}\text{I}$ ] labeled benzamides [ $^{123}\text{I}$ ]N-(2-diethylaminoethyl)-4-iodobenzamide ([ $^{123}\text{I}$ ]BZA, **1**)<sup>11,12</sup> and [ $^{123}\text{I}$ ]N-(2-diethylaminoethyl)-2-iodobenzamide ([ $^{123}\text{I}$ ]BZA<sub>2</sub>, **2**)<sup>13,14</sup> (Figure 1) found cell uptake to be dependent on melanin content.<sup>15</sup> Subsequent single-photon emission computed tomography (SPECT) evaluation in patients demonstrated a high affinity and selectivity in imaging cutaneous and ocular melanoma deposits.<sup>11,14,16,17</sup> The substitution of the benzamide moiety in **1** and **2** for a nicotinamide moiety was performed in [ $^{123}\text{I}$ ]MEL008 (**3**) to enhance hydrophilicity and rapid clearance via renal excretion.<sup>18</sup>

Other molecules reported to show in vivo selectivity for melanin are those with various (hetero)aromatic systems.<sup>10,19</sup> These melanin binding molecules that are taken up by the tumor cells are not receptor mediated and do not directly participate in the melanin biosynthesis pathway.<sup>18</sup> As a

Received: May 21, 2015

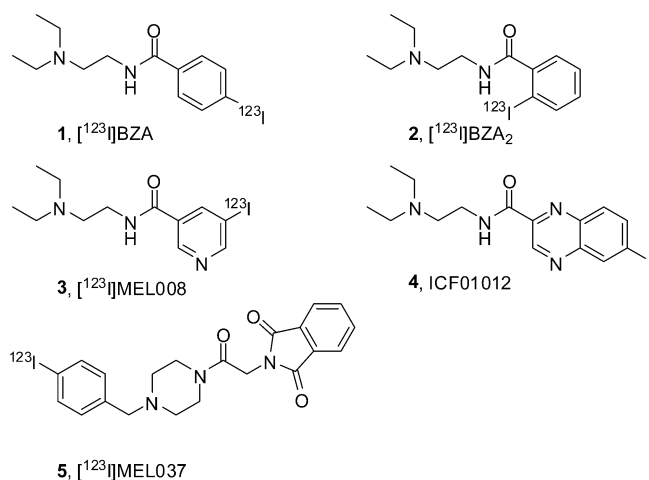


**Figure 1.** Chemical structures of various radiotracers with melanin specificity.

consequence, they do not appear to be transported into the cell through any known active transporter.<sup>10,18,20,21</sup> Although not completely understood, a factor that may be responsible for these types of compounds having high uptake into melanin expressing tumors could include a component of radiotracer bound to melanin and hence not released from the cell.

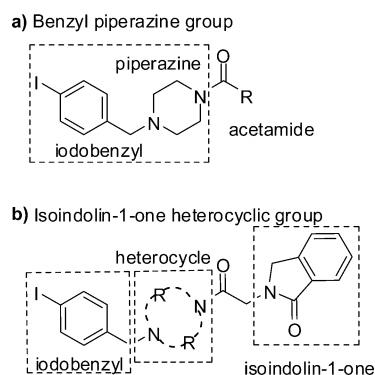
These types of analogues were found to bind to melanin expressing tumors with high specificity and moderate-to-high affinity in mice; particularly ICF01012 ([<sup>125</sup>I]4, Figure 1) displayed highly specific and long-lasting uptake in the tumor.<sup>10</sup> Furthermore, [<sup>131</sup>I], [<sup>123</sup>I] labeled,<sup>22</sup> and multimodal [<sup>18</sup>F]/[<sup>131</sup>I] labeled<sup>23</sup> analogues of 4 have shown suppression in B16F0<sup>23</sup> and SK-MEL-3<sup>22,24</sup> tumor bearing mice. This further validated the potential of these types of compounds for therapeutic applications of metastatic melanoma and hence led our research group to the development of [<sup>123</sup>I]MEL037 (5, Figure 1), which demonstrated high and prolonged tumor uptake, rapid whole body clearance, and potential therapeutic application.<sup>25</sup>

The structural modifications undertaken for 5 included a benzyl substituent (for straightforward radiolabeling via the stannyl precursor), the incorporation of stable functional groups (piperazine center)<sup>26</sup> into the amide, as well as the replacement of the benzamide/nicotinamide with an isoindolin-1,3-dione (phthalimide) to produce a more rigid and in vivo stable molecule.<sup>27</sup> Studies demonstrated 5 to have a 3-fold higher tumor uptake than 2, with rapid whole body clearance;<sup>27</sup> however, further preclinical evaluation of [<sup>131</sup>I]5 found the compound did not show the longitudinal in vivo stability required to be a suitable therapeutic agent.<sup>28</sup> This was postulated to be due to instability of the phthalamide group and provided the rationale for the work developed herein utilizing the isoindolin-1-one moiety. We report the development of a new class of melanin targeted agents, based on systematic structural variations of 1–5, as potential [<sup>131</sup>I] radiopharmaceuticals for treatment of malignant melanoma. Presented is the chemical synthesis, [<sup>123</sup>I] radiolabeling, and initial biological evaluation of these compounds.

## RESULTS AND DISCUSSION

**Chemistry.** In an effort to develop melanin specific radiotracers with improved in vivo stability, tumor uptake, and clearance from radiosensitive organs, we have pursued two

main subgroups based on the structures of 1–5: the benzylpiperazine group and the isoindolin-1-one heterocyclic group (Figure 2).

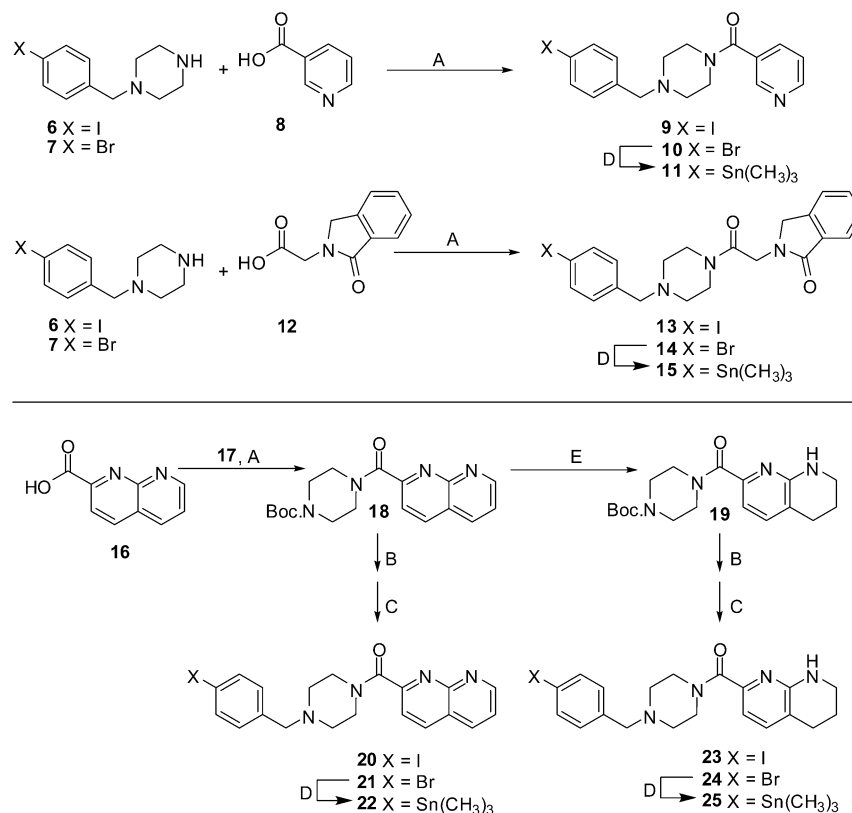


**Figure 2.** General structure of compounds containing (a) the iodinated benzylpiperazine group and (b) the isoindolin-1-one heterocyclic group of compounds synthesized in this study.

For the first group of new compounds synthesized (Figure 2a), the benzylpiperazine moiety (of 5) was maintained because of its known stability and ease of radioiodination.<sup>27</sup> The carboxylic acids for forming the acetamide were selected based on structures identified in the previously discussed compounds (Figure 1).<sup>10–14,18,25</sup> This included the nicotinamide group found in 3, 1,8-naphthyridin-2-yl based compounds, which are structurally similar to the quinoxalin-2-yl group found in 4, and the isoindolin-1-one group similar to 5. Synthesis of these compounds was achieved using standard literature coupling conditions (HOBt, EDC, DIPEA) that were used previously for the synthesis of similar compounds.<sup>18,25,27</sup> Commercially available 4-iodobenzylpiperazine (6) (for synthesis of iodinated nonradioactive standards) or 4-bromobenzylpiperazine (7) (for synthesis of brominated compounds) was condensed with nicotinic acid (8) to yield 9–10 and separately with 2-(1-oxoisoindolin-2-yl)acetic acid (12) to yield 13 and 14 (Scheme 1, top). 13 and 14 (which contain both benzylpiperazine and the isoindolin-1-one heterocyclic group) belong to both synthetic subgroups but have been categorized with the compounds of the benzylpiperazine group (Figure 2a) because of the similar synthetic method.

Alternatively, synthesis of other analogues in the benzylpiperazine group (the 1,8-naphthyridine and partially reduced 1,8-naphthyridine moiety) proceeded via a convergent pathway (Scheme 1, bottom). The 1,8-naphthyridine moiety was chosen, as it is similar in structure to literature standard 4 except that the positions of the nitrogen atoms in the aromatic ring are modified. The 1,8-naphthyridine moiety also gave easy one-step access to the partially reduced moiety, readily producing two compounds with different lipophilicity and  $\pi$ -stacking characteristics for comparison. 1,8-Naphthyridine-2-carboxylic acid (16) coupled to 1-Boc-piperazine (17), which allowed access to the key Boc-protected intermediate 18, then was reduced with Pd/C under H<sub>2(g)</sub> atmosphere to yield 19. Subsequent Boc-deprotection of 18 and 19 with trifluoroacetic acid (TFA) (isolated as the free amine) followed by N-alkylation with 4-bromo or 4-iodobenzyl bromide afforded iodinated standards and brominated compounds 20–21, and 23–24, respectively (Scheme 1, bottom).

In the second group of compounds (isoindolin-1-one heterocycles, Figure 2b), the isoindolin-1-one (of 13–15)

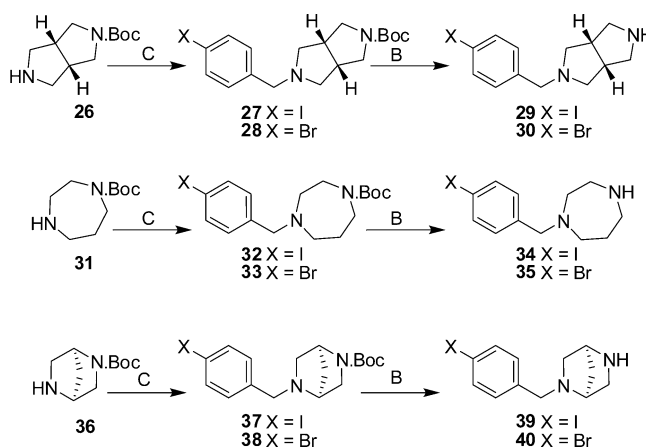
Scheme 1. Synthesis of Iodo-, Bromo-, and Stannybenzylpiperazine Derivatives<sup>a</sup>

<sup>a</sup>Reagents and conditions: (A) HOBt, EDC, DIPEA, DMF, 16 h, rt; (B) TFA, CH<sub>2</sub>Cl<sub>2</sub>, 16 h, rt; (C) 4-iodo or 4-bromobenzyl bromide, K<sub>2</sub>CO<sub>3</sub>, CH<sub>3</sub>CN, 16 h, reflux; (D) Sn<sub>2</sub>(CH<sub>3</sub>)<sub>6</sub>, Pd(PPh<sub>3</sub>)<sub>4</sub>, toluene, 16 h, 80 °C; (E) Pd/C, H<sub>2</sub>(g), EtOH, 16 h, rt.

and benzyl moiety of the first group were retained; however, the piperazine central linker was modified with four heterocyclic amines. The four heterocycles chosen are all structural modifications of the piperazine core, known for its stability,<sup>27</sup> to observe what effect this change to stability, flexibility/rigidity would have on the in vivo behavior of the molecules.

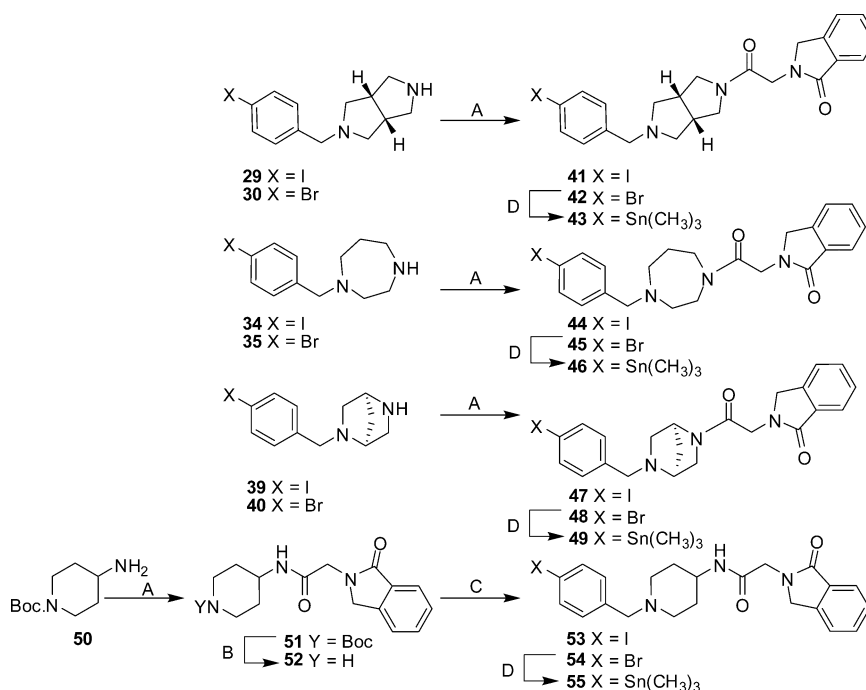
The synthesis began with the corresponding Boc protected intermediates (26, 31, 36), which were *N*-alkylated with either 4-iodo or 4-bromobenzyl bromide to give 27–28, 32–33, and 37–38 followed by Boc-deprotection with TFA and isolation as the free amine as described in Scheme 2. The resulting amines (29–30, 34–35, 39–40) were coupled with 2-(1-oxoisindolin-2-yl)acetic acid (12) to yield iodinated and brominated compounds 41–42, 44–45, 47–48, respectively (Scheme 3). The iodinated standard 53 and brominated compound 54 were synthesized via an alternative method, as 4-amino-1-Boc-piperidine hydrochloride (50) was commercially available. 12 was first coupled to 50 to give 51, followed by Boc-deprotection with TFA, which was isolated as the free amine 52, that was then *N*-alkylated with 4-iodo or 4-bromobenzyl bromide to give compounds 53–54 (Scheme 3).

Brominated compounds (10, 14, 21, 24, 42, 45, 48, 54) and the literature nonradioactive iodinated standard 4 were each individually treated with hexamethylditin and a catalytic amount of tetrakis(triphenylphosphine)palladium(0) (Pd(PPh<sub>3</sub>)<sub>4</sub>) to yield the stannyl radiolabeling precursors (11, 15, 22, 25, 43, 46, 49, 55 (Schemes 1 and 3) and literature 56 (Supporting Information) for use in electrophilic [<sup>125</sup>I] radioiodination.

Scheme 2. Synthesis of Intermediates from the Isoindolin-1-one Heterocyclic Group<sup>a</sup>

<sup>a</sup>Reagents and conditions: (C) 4-iodo or 4-bromobenzyl bromide, K<sub>2</sub>CO<sub>3</sub>, CH<sub>3</sub>CN, 16 h, reflux; (B) TFA, CH<sub>2</sub>Cl<sub>2</sub>, 16 h, rt.

<sup>1</sup>H NMR spectra of compounds in the isoindolin-1-one group were generally more complicated than their simple benzylpiperazine analogues, predominantly because of either conformational restriction or “potential” conformational flexibility in concert with amide isomerism. Despite the complex NMR spectra, complete characterization was possible, details of which and associated spectra can be found in the Supporting Information (Figure S1).

Scheme 3. Synthesis of Compounds Containing the Heterocyclic Isoindolin-1-one Group<sup>a</sup>

<sup>a</sup>Reagents and conditions: (A) **12**, HOBT, EDC, DIPEA, DMF, 16 h, rt; (B) TFA, CH<sub>2</sub>Cl<sub>2</sub>, 16 h, rt; (C) 4-iodo or 4-bromobenzyl bromide, K<sub>2</sub>CO<sub>3</sub>, CH<sub>3</sub>CN, 16 h, reflux; (D) Sn<sub>2</sub>(CH<sub>3</sub>)<sub>6</sub>, Pd(PPh<sub>3</sub>)<sub>4</sub>, toluene, 16 h, 80 °C.

Table 1. [<sup>123</sup>I] Radiolabeling and Purification Conditions

radiotracer	precursor	HPLC mobile phase (CH <sub>3</sub> CN/H <sub>2</sub> O/modifier)	retention time (min) <sup>a</sup>	radiochemical yield (%)
[ <sup>123</sup> I] <b>9</b>	<b>11</b>	50:40:10 <sup>b,d</sup>	16.0	77.0 ± 6.2 (n = 3)
[ <sup>123</sup> I] <b>13</b>	<b>15</b>	50:40:10 <sup>b,d</sup>	17.3	83.3 ± 10.0 (n = 3)
[ <sup>123</sup> I] <b>20</b>	<b>22</b>	50:40:10 <sup>d,e</sup>	12.2	75.5 ± 3.5 (n = 2)
[ <sup>123</sup> I] <b>23</b>	<b>25</b>	25:65:10 <sup>c,e</sup>	16.6	68.8 ± 11.9 (n = 3)
[ <sup>123</sup> I] <b>41</b>	<b>43</b>	55:35:10 <sup>b,d</sup>	16.7	76.7 ± 2.1 (n = 3)
[ <sup>123</sup> I] <b>44</b>	<b>46</b>	55:35:10 <sup>b,d</sup>	14.5	76.0 ± 4.6 (n = 3)
[ <sup>123</sup> I] <b>47</b>	<b>49</b>	50:40:10 <sup>b,d</sup>	15.9	89.5 ± 2.1 (n = 3)
[ <sup>123</sup> I] <b>53</b>	<b>55</b>	30:60:10 <sup>d,e</sup>	14.8	58.7 ± 5.9 (n = 3)
[ <sup>123</sup> I] <b>4</b>	<b>56</b>	50:40:10 <sup>b,c</sup>	15.7	73.3 ± 3.8 (n = 3)

<sup>a</sup>Flow at 2 mL/min. <sup>b</sup>0.1 M NH<sub>4</sub>HCO<sub>3</sub>, pH 8. <sup>c</sup>Waters Xterra 10 μm, 300 mm × 100 mm. <sup>d</sup>Phenomenex Bondclone 10 μm, 300 mm × 7.8 mm. <sup>e</sup>1% trifluoroacetic acid.

**Radiochemistry.** Radioiodination was achieved by reacting the stannyl precursor with [<sup>123</sup>I]Na via standard electrophilic iododestannylation chemistry in the presence of chloramine-T as the oxidant to afford the corresponding [<sup>123</sup>I] analogues. The [<sup>123</sup>I] labeled radiotracers were partially purified by solid phase extraction using a C18 Sep-Pak Light cartridge prior to reverse phase (RP)-HPLC purification to yield [<sup>123</sup>I] labeled radiotracers for all biological evaluations of radiochemical purity of >95%. Radiotracers were labeled in moderate-to-high radiochemical yields (60–90%) (Table 1). Specific activity was estimated to be >2 GBq/nmol based on the limit of detection of the HPLC system.

**SPECT Imaging Studies.** The eight new radiotracers ([<sup>123</sup>I]**9**, [<sup>123</sup>I]**13**, [<sup>123</sup>I]**20**, [<sup>123</sup>I]**23**, [<sup>123</sup>I]**41**, [<sup>123</sup>I]**44**, [<sup>123</sup>I]**47**, and [<sup>123</sup>I]**53**) as well as the literature radiotracer [<sup>123</sup>I]**4** were subjected to in vivo whole-body distribution monitoring over 72 h using SPECT imaging in C57BL/6J mice bearing the B16F0 murine melanoma tumor. This time frame was chosen to evaluate the potential [<sup>131</sup>I] therapeutic application of the radiotracers. The SPECT imaging studies were performed to

select the most promising radiotracers for further in vivo evaluation. Selection criteria included high and prolonged tumor uptake over time (expressed as the remained radioactivity (dpm) with decay correction) and high tumor-to-background (lungs) ratio (Table S1) indicating fast clearance from nontarget organs, in comparison to [<sup>123</sup>I]**4**. An example of a typical SPECT planar image of the distribution in this study is shown in Figure 3 ([<sup>123</sup>I]**41**), and the entire range of SPECT images is available in the Supporting Information (Figure S2).

Several radiotracers experienced high thyroid uptake (in vivo deiodination) including [<sup>123</sup>I]**44** and [<sup>123</sup>I]**47** at 72 h and [<sup>123</sup>I]**9** from 24 h onward. [<sup>123</sup>I]**4** displayed significant thyroid uptake visible from 3 h postinjection and also appeared to enter the brain from early time points scans (prior to 1 h). Over the study time period, unlike [<sup>123</sup>I]**4**, no localization of radioactivity was observed in the brain for the eight new radiotracers, indicating that they did not cross the blood–brain barrier. For animals involved in the study of [<sup>123</sup>I]**20**, the scans at longer time points (48–72 h) could not be performed because of the ethical restrictions on the tumor growth and permissible size.

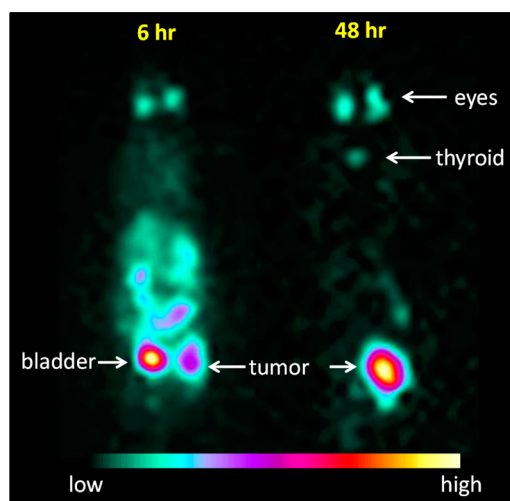


**Figure 3.** Representative planar SPECT image of the distribution of  $[^{123}\text{I}]\mathbf{41}$  in C57BL/6J black mouse bearing B16F0 murine melanoma tumor.

For all new radiotracers tested, radioactive signal was observed in the eyes, which supported the specific uptake in melanin-rich tissues; however, the study was conducted in C57BL/6J mice that have high melanin pigmentation in the eyes<sup>27,29</sup> (as well as skin, hair, and spleen).<sup>30–33</sup> Because of the large differences between murine and human ocular geometry as well as uveal melanin content, radioactivity uptake in the eyes may not be an issue for clinical transfer.<sup>19</sup> Additionally, the first in human study of a similar benzamide-type radiotracer developed by our research group ( $[^{18}\text{F}]\text{MEL050}$ )<sup>34,35</sup> indicated that the radiotracer is safe with suitable biodistribution for PET imaging.<sup>36</sup>

Figure 4a shows the tumor-to-background ratios (TBRs) of all studied radiotracers. For the period of 24–72 h all radiotracers (except  $[^{123}\text{I}]\mathbf{9}$ ) clearly possessed higher uptake ratios compared to that of  $[^{123}\text{I}]\mathbf{4}$ .  $[^{123}\text{I}]\mathbf{13}$ ,  $[^{123}\text{I}]\mathbf{44}$ , and  $[^{123}\text{I}]\mathbf{47}$  displayed a fast tumor wash-out compared to the remaining new radiotracers; however, the TBRs were still greater than  $[^{123}\text{I}]\mathbf{4}$  at 72 h.

Figure 4b demonstrates the tumor kinetic profiles of the studied radiotracers which are expressed as decay-corrected radioactivity retained in the tumor over time. Tumor kinetic profiles were utilized, as they are more representative in terms of indicating the dynamic process of the radiotracer uptake into the target and its clearance from the body or from nontarget tissues over time. In comparison, for example, tumor-uptake profiles present the static uptake ratios (tumor-to-organ) only at a particular time point. At time point 24 h,  $[^{123}\text{I}]\mathbf{13}$ ,  $[^{123}\text{I}]\mathbf{20}$  (see Figure 4 caption about  $[^{123}\text{I}]\mathbf{20}$ ),  $[^{123}\text{I}]\mathbf{23}$ ,  $[^{123}\text{I}]\mathbf{41}$ , and  $[^{123}\text{I}]\mathbf{53}$  had higher tumor uptake compared to  $[^{123}\text{I}]\mathbf{4}$ ; however, at 48 h only  $[^{123}\text{I}]\mathbf{41}$  and  $[^{123}\text{I}]\mathbf{53}$  demonstrated higher tumor uptake than  $[^{123}\text{I}]\mathbf{4}$ . At 72 h only  $[^{123}\text{I}]\mathbf{53}$  displayed higher tumor uptake than  $[^{123}\text{I}]\mathbf{4}$ . Although SPECT imaging could not be obtained for  $[^{123}\text{I}]\mathbf{20}$  after 24 h because of ethical restrictions, the radiotracer initially showed great potential and may have continued to if the trend (Figure 4) remained as anticipated. On the basis of these results, the most favorable radiotracers ( $[^{123}\text{I}]\mathbf{20}$ ,  $[^{123}\text{I}]\mathbf{23}$ ,  $[^{123}\text{I}]\mathbf{41}$ , and  $[^{123}\text{I}]\mathbf{53}$ ) were selected for further in vivo biological investigation (biodistribution and metabolite studies) for evaluation as potential  $[^{131}\text{I}]$  therapeutic agents.

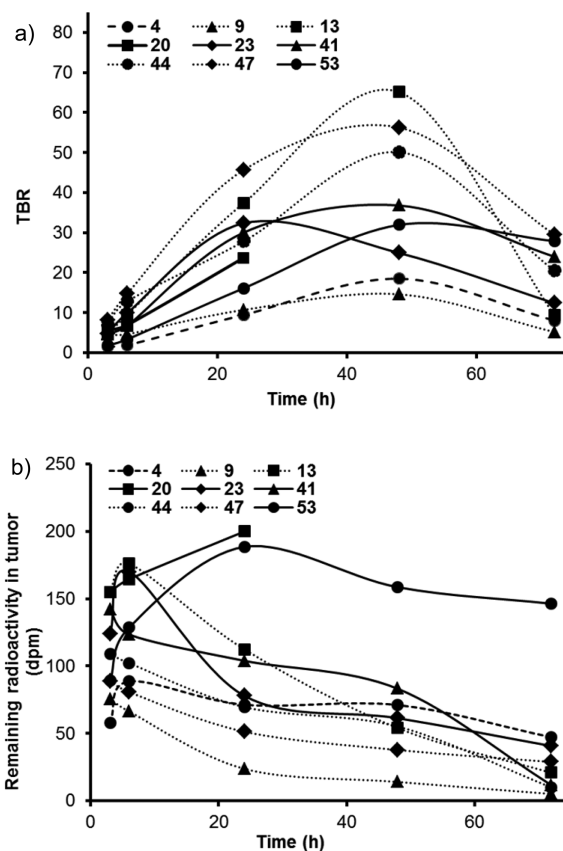


**Figure 4.** Comparison of (a) tumor-to-background (TBR) uptake ratios and (b) tumor kinetic profiles over time of  $[^{123}\text{I}]$  labeled compounds in C57BL/6J black mice bearing B16F0 murine melanoma tumor. Full tabulated data can be found in the [Supporting Information](#) (Table S1). For animals involved in the study of  $[^{123}\text{I}]\mathbf{20}$ , the scans at longer time points (48–72 h) could not be performed because of the ethical restrictions on the tumor growth and permissible size.

**Biodistribution Studies.** Radiotracers  $[^{123}\text{I}]\mathbf{20}$ ,  $[^{123}\text{I}]\mathbf{23}$ ,  $[^{123}\text{I}]\mathbf{41}$ , and  $[^{123}\text{I}]\mathbf{53}$  were injected into B16F0 tumor bearing C57BL/6J mice to evaluate the potential of their corresponding  $[^{131}\text{I}]$  labeled analogues as melanotic tumor therapeutics. Criteria to assess their potential therapeutic properties included high and prolonged tumor uptake (indicating high affinity and specificity for melanotic tissues), high tumor-to-radiosensitive organ areas under the curves ratios (AUCRs) (indicating high cumulative uptake in the tumor, yet low cumulative uptake in radiosensitive organs), low thyroid uptake (indicating low in vivo deiodination), and the amount of intact radiotracer in the tumor (indicating in vivo stability).

Postinjection time points at 1, 3, 6, 16, 24, and 48 h were selected to determine the distribution of each compound in various tissues. Longer time points of 16, 24, and 48 h were included to determine the long-term retention of the radiotracers in the body. The values of tumor and representative organ radioactivity concentration, expressed in percent of injected dose per gram (% ID/g), are presented in [Table 2](#) and additional values for all organs measured are detailed in the [Supporting Information](#) (Table S2).

High uptake in the liver was observed for all four radiotracers (16–42% at 1 h,  $[^{123}\text{I}]\mathbf{41} > [^{123}\text{I}]\mathbf{23} > [^{123}\text{I}]\mathbf{20} > [^{123}\text{I}]\mathbf{53}$ ), suggesting an involvement of the clearance via the hepatic portal pathway. By 16 h, the liver uptake of all radiotracers was reduced to background level. The estimated biological half-lives

**Table 2. Distribution (% ID/g Organ  $\pm$  SEM,  $n = 5$ ) in Selected Organs<sup>a</sup> of [<sup>123</sup>I]20, 23, 41, and 53 in C57BL/6J Mice Grafted with F0 Melanoma Tumor (Decay Corrected)**

compd	time (h)	tumor	eyes	large GIT	small GIT	thyroid	spleen <sup>b</sup>	liver	kidney
[ <sup>123</sup> I]20	1	17.1 $\pm$ 2.8	32.0 $\pm$ 1.2	3.2 $\pm$ 0.2	14.4 $\pm$ 0.8	2.3 $\pm$ 0.1	2.6–8.6	15.9 $\pm$ 0.8	7.5 $\pm$ 0.5
	3	20.0 $\pm$ 2.8	36.0 $\pm$ 2.4	11.9 $\pm$ 1.6	14.1 $\pm$ 0.9	2.2 $\pm$ 0.5	2.3–13.3	13.4 $\pm$ 0.8	6.2 $\pm$ 0.4
	6	19.4 $\pm$ 2.6	37.2 $\pm$ 1.7	18.6 $\pm$ 2.1	6.1 $\pm$ 0.9	3.5 $\pm$ 0.5	2.1–16.7	10.1 $\pm$ 0.3	5.2 $\pm$ 0.4
	16	18.4 $\pm$ 1.1	32.9 $\pm$ 2.4	1.8 $\pm$ 0.1	1.3 $\pm$ 0.1	1.6 $\pm$ 0.2	0.8–3.4	2.4 $\pm$ 0.2	1.6 $\pm$ 0.1
	24	14.4 $\pm$ 1.0	35.1 $\pm$ 3.4	1.4 $\pm$ 0.2	0.9 $\pm$ 0.05	2.9 $\pm$ 1.3	0.5–3.4	1.8 $\pm$ 0.1	1.4 $\pm$ 0.02
	48	13.1 $\pm$ 3.9	31.6 $\pm$ 1.2	0.3 $\pm$ 0.02	0.2 $\pm$ 0.02	5.3 $\pm$ 0.9	0.2–4.9	0.7 $\pm$ 0.04	0.5 $\pm$ 0.04
[ <sup>123</sup> I]23	1	19.2 $\pm$ 1.0	40.3 $\pm$ 2.8	7.9 $\pm$ 0.4	45.6 $\pm$ 3.9	5.1 $\pm$ 0.4	3.5–24.4	19.5 $\pm$ 0.7	15.6 $\pm$ 1.3
	3	32.1 $\pm$ 2.3	56.4 $\pm$ 5.4	59.6 $\pm$ 10.4	63.8 $\pm$ 4.2	2.7 $\pm$ 0.1	2.0–7.3	13.2 $\pm$ 0.5	9.0 $\pm$ 0.6
	6	32.5 $\pm$ 1.4	52.8 $\pm$ 5.8	87.1 $\pm$ 3.9	11.5 $\pm$ 0.7	2.7 $\pm$ 0.5	1.0–1.9	6.3 $\pm$ 0.6	10.0 $\pm$ 5.1
	16	20.4 $\pm$ 2.6	28.6 $\pm$ 1.3	2.3 $\pm$ 0.2	1.4 $\pm$ 0.1	2.5 $\pm$ 0.5	0.3–4.0	0.9 $\pm$ 0.1	1.2 $\pm$ 0.1
	24	12.9 $\pm$ 1.4	30.8 $\pm$ 1.4	1.7 $\pm$ 0.3	0.8 $\pm$ 0.1	2.0 $\pm$ 0.4	0.2–2.4	0.8 $\pm$ 0.05	1.0 $\pm$ 0.1
	48	5.6 $\pm$ 0.9	19.0 $\pm$ 1.1	0.2 $\pm$ 0.04	0.1 $\pm$ 0.02	2.1 $\pm$ 0.4	0.05–0.3	0.2 $\pm$ 0.01	0.4 $\pm$ 0.02
[ <sup>123</sup> I]41	1	10.3 $\pm$ 2.5	18.2 $\pm$ 4.1	3.5 $\pm$ 0.8	21.4 $\pm$ 4.9	1.9 $\pm$ 0.5	0.2–9.8	12.3 $\pm$ 0.8	15.8 $\pm$ 3.6
	3	10.8 $\pm$ 1.6	18.5 $\pm$ 4.7	21.4 $\pm$ 2.3	15.2 $\pm$ 0.6	1.5 $\pm$ 0.2	0.5–5.6	5.6 $\pm$ 0.2	8.4 $\pm$ 0.2
	6	10.4 $\pm$ 0.9	21.8 $\pm$ 2.0	23.1 $\pm$ 2.3	2.6 $\pm$ 0.2	2.8 $\pm$ 0.4	0.4–4.1	3.1 $\pm$ 0.1	4.1 $\pm$ 0.2
	16	11.6 $\pm$ 1.6	22.1 $\pm$ 1.4	1.4 $\pm$ 0.2	0.5 $\pm$ 0.04	1.0 $\pm$ 0.4	0.2–5.1	0.7 $\pm$ 0.05	1.0 $\pm$ 0.1
	24	7.8 $\pm$ 1.6	18.4 $\pm$ 0.9	1.0 $\pm$ 0.1	0.3 $\pm$ 0.04	1.0 $\pm$ 0.3	0.05–3.4	0.4 $\pm$ 0.04	0.5 $\pm$ 0.1
	48	5.0 $\pm$ 0.7	15.8 $\pm$ 0.7	0.1 $\pm$ 0.01	0.1 $\pm$ 0.004	3.4 $\pm$ 1.7	0.09–3.0	0.2 $\pm$ 0.01	0.2 $\pm$ 0.01
[ <sup>123</sup> I]53	1	6.2 $\pm$ 0.8	13.7 $\pm$ 0.5	6.6 $\pm$ 0.3	11.9 $\pm$ 0.9	3.4 $\pm$ 0.2	9.6–12.6	41.8 $\pm$ 1.0	8.0 $\pm$ 0.5
	3	11.6 $\pm$ 0.8	20.8 $\pm$ 0.6	10.9 $\pm$ 0.4	12.0 $\pm$ 0.5	3.4 $\pm$ 0.1	7.6–16.9	38.8 $\pm$ 1.1	7.4 $\pm$ 0.2
	6	18.1 $\pm$ 10.0	28.1 $\pm$ 2.5	17.6 $\pm$ 1.0	9.8 $\pm$ 0.7	3.1 $\pm$ 0.2	3.6–17.7	35.1 $\pm$ 3.0	5.0 $\pm$ 0.7
	16	18.1 $\pm$ 2.0	40.4 $\pm$ 3.0	8.1 $\pm$ 0.9	3.7 $\pm$ 0.3	2.3 $\pm$ 0.2	1.3–17.3	7.1 $\pm$ 0.3	1.8 $\pm$ 0.1
	24	15.2 $\pm$ 3.8	41.4 $\pm$ 2.3	8.0 $\pm$ 1.2	3.8 $\pm$ 0.3	2.6 $\pm$ 0.3	1.2–17.8	7.8 $\pm$ 0.6	1.9 $\pm$ 0.2
	48	13.2 $\pm$ 4.3	38.7 $\pm$ 3.1	0.6 $\pm$ 0.05	0.3 $\pm$ 0.03	2.4 $\pm$ 0.3	0.1–2.0	1.9 $\pm$ 0.2	0.3 $\pm$ 0.03

<sup>a</sup>Table of organ distribution in all organs can be found in Supporting Information, Table S2. <sup>b</sup>% ID/g in spleen are presented as range of values because of differences in the extent of pigmentation of the spleen.<sup>10</sup>

were based on the biodistribution profile of the four tracers in the liver and kidney, as the main route of metabolism and excretion, respectively. The estimated biological half-lives for [<sup>123</sup>I]41 and [<sup>123</sup>I]23 were 3–6 h and 6–16 h for [<sup>123</sup>I]20 and [<sup>123</sup>I]53. The kidneys displayed low-to-medium uptake, ~16% ID/g at 1 h for [<sup>123</sup>I]23 and [<sup>123</sup>I]41 and ~8% ID/g at 1 h for [<sup>123</sup>I]20 and [<sup>123</sup>I]53, all of which decreased to background level by 16 h. Thyroid uptake was low for all radiotracers and generally plateaued at ~3% ID/g across all time points, indicating minor amounts of in vivo deiodination. Generally, uptake in the GIT (small and large) was low for all radiotracers, peaking at 3–6 h (~17% ID/g) and decreasing to background levels over time except for [<sup>123</sup>I]23 which initially showed very high uptake (large GIT 87% ID/g at 6 h and small GIT 64% ID/g at 3 h) and then continued to decrease to background level over time.

For all radiotracers tested, high radioactivity uptake was observed in melanin containing tissues (i.e., tumor, eyes, and spleen). In the tumor, [<sup>123</sup>I]23 exhibited the highest uptake (33% ID/g at 6 h) but significantly decreased with time, whereas high and prolonged tumor uptake was observed for [<sup>123</sup>I]20 and [<sup>123</sup>I]53 (13% ID/g at 48 h). High and prolonged eye uptake was observed for all radiotracers (at least 16% ID/g at 48 h); again [<sup>123</sup>I]23 exhibited the highest uptake (56% ID/g at 3 h) and then significantly decreased with time. The spleen displayed a varied range of radioactive uptake for all radiotracers tested, from background level to a peak at 24% ID/g ([<sup>123</sup>I]20 at 1 h). This result was not unexpected because of large differences in the extent of pigmentation of the spleen (splenic melanosis) found in black mice, particularly the C57BL/6J strain.<sup>31,32</sup> This is a normal condition that can be found in various organs but most commonly the spleen where

part or all of the spleen is heavily pigmented and can also display interindividual variation.<sup>30,33</sup>

Whole body clearance (>98% of injected activity) was observed for each tracer at 16 h postinjection (Figure 5). These

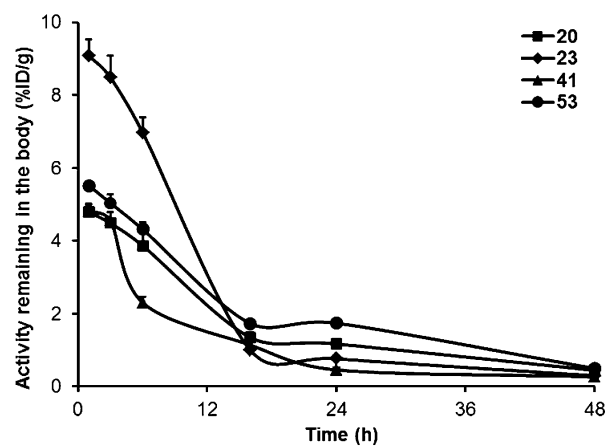


**Figure 5.** Activity remaining in the body (% ID/g  $\pm$  SEM  $n = 5$ , decay corrected) at various time points postinjection of the four [<sup>123</sup>I] radiotracers in C57BL/6J black mice with B16F0 tumors. Data were obtained from the biodistribution studies.

data re-enforced the findings from the initial SPECT studies which supported a melanin-related uptake mechanism with a high selectivity and specificity for melanin content.

In order to evaluate the therapeutic potential of these radiotracers, their nonstochastic effects have to be considered. The therapeutic potential of a radiotracer is indicated by a high cumulative uptake in the tumor (tumor AUCs), a low

Table 3. Area under the Curve (AUC) of Lead [<sup>123</sup>I] Labeled Compounds in Radiosensitive Organs<sup>a</sup>

compd	radiosensitive organ AUC (% ID g <sup>-1</sup> h <sup>-1</sup> )					
	tumor	skin	eyes	bone	GIT	thyroid
[ <sup>123</sup> I]20	746.8 ± 61.9	16.6 ± 0.4	1601.4 ± 72.0	19.0 ± 4.1*	136.5 ± 8.0*	154.3 ± 18.1
[ <sup>123</sup> I]23	768.1 ± 24.9	24.4 ± 7.5	1501.4 ± 73.1	12.3 ± 1.3	428.8 ± 15.3	107.6 ± 5.7
[ <sup>123</sup> I]41	716.7 ± 107.7	32.7 ± 4.8	1737.4 ± 53.4	29.0 ± 2.0	246.2 ± 11.4	122.2 ± 8.0
[ <sup>123</sup> I]53	396.0 ± 27.0*	18.2 ± 2.8	904.9 ± 28.3*	6.1 ± 0.3**	135.8 ± 7.3*	90.4 ± 25.9

<sup>a</sup>Data are derived from the biodistribution studies and presented as the mean of the ratios ± SEM, *n* = 5. Areas under the curves are calculated using GraphPad Prism, version 5.04. One-way ANOVA (radiotracers as factor), followed by Bonferroni post hoc tests. \*0.01 < *P* < 0.05. \*\**P* < 0.001.

Table 4. Tumor-to-Radiosensitive Organ Area under the Curve Ratios (AUCRs) of Lead [<sup>123</sup>I] Labeled Compounds<sup>a</sup>

compd	tumor-to-radiosensitive organ AUC ratio				
	tumor/skin	tumor/eyes	tumor/bone	tumor/GIT	tumor/thyroid
[ <sup>123</sup> I]20	45.3 ± 4.2	0.47 ± 0.03	44.0 ± 7.0	5.5 ± 0.4**	5.0 ± 0.5
[ <sup>123</sup> I]23	40.9 ± 8.1	0.52 ± 0.02	65.5 ± 8.2	1.8 ± 0.03	7.2 ± 0.3
[ <sup>123</sup> I]41	23.1 ± 4.5	0.42 ± 0.07	25.0 ± 3.8***	2.9 ± 0.4	6.0 ± 1.1
[ <sup>123</sup> I]53	24.4 ± 5.2	0.44 ± 0.04	65.8 ± 5.2	3.0 ± 0.4	5.8 ± 1.4

<sup>a</sup>One-way ANOVA (radiotracers as factor), followed by Bonferroni post hoc tests. \*\*\**P* < 0.001. \*\**P* < 0.01.

cumulative uptake in the radiosensitive organs (radiosensitive organ AUCs, Table 3), and a high ratio of the two uptakes (tumor-to-radiosensitive organ AUCRs, Table 4). Radiosensitive organs such as the gastrointestinal tract (stomach, small and large intestines), skin, eyes, bone marrow, and thyroid<sup>18</sup> were selected for calculation of tumor-to-organ cumulative uptake (% ID/g) over time ratios (AUCRs) and served as a direct indication of the potential absorbed dose of the radiotracer to the radiosensitive organs and indirectly their therapeutic potential (Table 4).

Statistical analysis of AUCRs was performed for each radiosensitive organ and each radiotracer. One-way ANOVA analysis of the time–activity areas under the curves (AUCs) for each radiosensitive organ among the radiotracers, with radiotracers as an independent factor, showed that the cumulative uptake in the tumor over time of [<sup>123</sup>I]20, [<sup>123</sup>I]23, and [<sup>123</sup>I]41 are significantly higher than that of [<sup>123</sup>I]53 ( $F_{3,16} = 7.319$ ,  $P = 0.0026$ ). However, there is no significant difference among these three radiotracers. [<sup>123</sup>I]53 showed lowest cumulative uptake over time in the eyes ( $0.01 < P < 0.05$ ), bone ( $P < 0.001$ ), and GIT ( $0.01 < P < 0.05$ ) compared to other radiotracers. Separate one-way ANOVA analyses for each of the tumor-to-radiosensitive organ AUCRs among the radiotracers indicated that there were no statistically significant difference between the tumor-to-skin, tumor-to-eyes, and tumor-to-thyroid AUCRs. However, there was an overall significant difference among the tumor-to-GIT AUCRs ( $F_{3,16} = 20.92$ ,  $P < 0.0001$ ) and tumor-to-bone AUCRs ( $F_{3,16} = 9.768$ ,  $P = 0.0007$ ) for these radiotracers. Bonferroni post hoc analysis indicated that [<sup>123</sup>I]23 had the highest tumor-to-GIT AUCR (i.e., lowest absorbed dose to the GIT,  $P < 0.001$ ), and both [<sup>123</sup>I]23 and [<sup>123</sup>I]53 had the highest tumor-to-bone AUCRs (i.e., lowest absorbed dose to bone,  $P < 0.01$ ) compared to other radiotracers.

**Metabolite Studies.** The in vivo stability of [<sup>123</sup>I]20, [<sup>123</sup>I]23, [<sup>123</sup>I]41, and [<sup>123</sup>I]53 were evaluated by radio-TLC and radio-HPLC analysis at 3 and 24 h postinjection in the tumor, eyes, spleen, urine, and plasma (Supporting Information Table S3). Overall, both analytical methods examined the retained radioactivity that was bound to a tissue corresponding to the intact radiotracer and yielded results in concordance with each other presenting similar trends of in vivo stability. The time

point of 24 h is particularly applicable to these radiotracers for their therapeutic potentials. In the tumor and eyes (melanin containing tissues), ~90% of the radioactive signal corresponded to intact tracers [<sup>123</sup>I]41 and [<sup>123</sup>I]53 (at 3 h) and showed prolonged stability over time (~80% at 24 h). Conversely, [<sup>123</sup>I]20 and [<sup>123</sup>I]23 showed poor in vivo stability in the tumor and eyes (~60% at 3 h, ~35% at 24 h). All tracers exhibited fast breakdown in the urine and plasma (mostly undetectable). These results demonstrated that once bound to melanin in pigmented tissues [<sup>123</sup>I]41 and [<sup>123</sup>I]53 remained highly unchanged. The extraction efficiencies for all tracers in all tissues and time points tested were found to be diverse (~60–90%) (Supporting Information Table S4) but are in accordance with other compounds of similar structure (5).<sup>25</sup>

## CONCLUSIONS

With the aim of developing new radiotherapeutics for use in metastatic melanoma, we have synthesized iodinated melanin targeting compounds containing either a benzylpiperazine or an isoindolin-2-one heterocyclic moiety. Eight new compounds and literature compound 4 were radiolabeled with [<sup>123</sup>I] and whole-body-imaged in B16F0 tumor bearing C57BL/6J mice using SPECT. All compounds displayed high and distinct uptake between targets and nontargets and good tumor-to-background ratio, compared with literature compound [<sup>123</sup>I]4.

The most favorable compounds from the SPECT study ([<sup>123</sup>I]20, [<sup>123</sup>I]23, [<sup>123</sup>I]41, and [<sup>123</sup>I]53) were further investigated by biodistribution and metabolite studies for their therapeutic potential against melanoma. [<sup>123</sup>I]20 and [<sup>123</sup>I]53 displayed the favorable pharmacokinetic properties in the biodistribution studies with clear delineation of the tumor as early as 1 h postinjection and prolonged tumor retention. Although [<sup>123</sup>I]53 appeared to have the lowest cumulative uptake in the tumor over time compared to other radiotracers, [<sup>123</sup>I]20 had the lowest absorbed dose to GIT; however, it had low stability. Both [<sup>123</sup>I]23 and [<sup>123</sup>I]53 had the lowest absorbed dose to bone. Metabolite analysis of [<sup>123</sup>I]41 and [<sup>123</sup>I]53 displayed high and prolonged amounts of intact tracer in melanin containing tissues. Results herein suggest that compound [<sup>123</sup>I]53 is an ideal candidate from this new series to proceed with further preclinical [<sup>131</sup>I] therapeutic evaluation.

## EXPERIMENTAL SECTION

### Materials for Chemical Synthesis and Radiochemistry.

Paraformaldehyde, *N*-benzylmaleimide, 1-chloroethyl chloroformate, homopiperazine, 1-Boc-piperazine (17), 4-iodobenzyl bromide, 4-bromobenzyl bromide, 1-(4-bromobenzyl)piperazine (7), 4-amino-1-Boc-piperidine hydrochloride (50), nicotinic acid (8), 2-(1-oxoisoin-dolin-2-yl)acetic acid (12), methyl pyruvate, 2-amino-3-pyridine carboxaldehyde, 6,7-dimethoxy-1,2,3,4-tetrahydroisoquinoline hydrochloride, benzyl bromoacetate, 2-carboxybenzaldehyde, glycine methyl ester hydrochloride, hexamethylditin, potassium iodide, Pd(PPh<sub>3</sub>)<sub>4</sub>, TFA, and chloramine-T hydrate (98%) were purchased from Sigma-Aldrich. Di-*tert*-butyl dicarbonate was purchased from Alfa Aesar. 1-(4-Iodobenzyl)piperazine (6) was purchased from ACB Blocks. All HPLC solvents were of HPLC grade and were filtered before use. All other reagents were of analytical grade or higher and used as received. Na<sup>123</sup>I no-carrier added was purchased as from ANSTO Health. Silica gel TLC plates with a preconcentration zone used in metabolite studies were purchased from Merck.

**Instrumentation.** Nuclear magnetic resonance (NMR) spectra were recorded using a Bruker Avance DPX-400 spectrometer operating at 400.13 MHz for <sup>1</sup>H NMR and at 100.61 MHz for <sup>13</sup>C NMR. Low-resolution mass spectrometry (LR-MS) was performed on a Micromass ZQ quadrupole mass spectrometer, and high-resolution mass spectrometry (HR-MS) was performed at the University of Wollongong, Australia, using a Bruker Daltonics BioApex-II 7T FTICR spectrometer equipped with an off-axis analytical electron spray ionization source.

All nonradioactive standards and radiolabeling precursors were purified by HPLC using a Waters XBridgeC18 100 mm × 30 mm column (unless specified otherwise), with flow rate at 20 mL/min under gradient conditions of (A) CH<sub>3</sub>CN, (B) H<sub>2</sub>O, (C) 100 mM pH 8 NH<sub>4</sub>HCO<sub>3</sub>. Detection wavelength was either 210 or 254 nm. Two systems were used for purification, either Waters PrepLC pump coupled with 717 autosampler and 486 UV detector or Waters 600 controller pump coupled with 717 autosampler and 996 photodiode array UV detector.

HPLC purity analysis was performed using a Waters Empower 2 system with a Waters 600 pump, Waters in-line degasser AF, Waters temperature control module II, Waters 717 autosampler, and Water 2996 PDA. Either an Alltech Alltima C18 (150 mm × 4.6 mm, 5 μm) or Waters XTerra RP (150 mm × 4.6 mm, 5 μm) analytical column was used, with absorbance measured at 210 or 254 nm. Samples were prepared as 1 mg/mL, with a 10 μL injection. Solvent conditions were as shown in Table 5.

**Table 5. HPLC Solvent Conditions**

entry	time	flow (mL/min)	% A		% C (100 mM NH <sub>4</sub> HCO <sub>3</sub> , pH 8, or 1% TFA/99% H <sub>2</sub> O)
			(CH <sub>3</sub> CN or CH <sub>3</sub> OH)	% B (H <sub>2</sub> O)	
1	0	1.00	10	80	10
2	20	1.00	90	0	10
3	21	1.00	10	80	10

Percentage purity of the iodinated standards and stannyl precursors were calculated from the area under the peak using Empower software (Waters). Preparative HPLC was conducted on nonradioactive iodinated standards and stannyl radiolabeling precursors to achieve purity of >95%.

**General Procedure A: Amide Coupling.** To a solution of the appropriate amine (1.0 equiv) in DMF (10 mL) were added 1-hydroxybenzotriazole hydrate (HOBt) (1.2 equiv), 1-(3-dimethylamino-propyl)-3-ethylcarbodiimide hydrochloride (EDC) (1.2 equiv), and diisopropylethylamine (DIPEA) (3 equiv), followed by the acid of interest (1.1 equiv, either purchased or synthesized). The reaction mixture was stirred under nitrogen for 16 h at rt, diluted with ethyl acetate (EtOAc) (50 mL), and washed with H<sub>2</sub>O, saturated NaHCO<sub>3(aq)</sub> and brine (3 × 20 mL, each). The organic phase was

dried over anhydrous Na<sub>2</sub>SO<sub>4</sub>, filtered, and evaporated under reduced pressure. The crude residue was purified by column chromatography (silica gel, 0–15% CH<sub>3</sub>OH/EtOAc), and the products were obtained as either a pale yellow oil or waxy solid. Full compound details are available in the [Supporting Information](#).

**General Procedure B: Amine Deprotection.** The desired Boc protected amine (~1 g) was stirred in TFA/CH<sub>2</sub>Cl<sub>2</sub> (1:4, 5 mL) for 16 h at rt. To isolate the product as the trifluoroacetate salt, the solvent was removed and the residue dissolved in CH<sub>2</sub>Cl<sub>2</sub>. To isolate as the free amine, the solution was first adjusted to pH 12 (with aqueous 1 M NaOH) before concentration and redissolution in CH<sub>2</sub>Cl<sub>2</sub>. It was then washed with brine (2 × 15 mL) and H<sub>2</sub>O (2 × 15 mL). The organic phase was dried over anhydrous Na<sub>2</sub>SO<sub>4</sub>, filtered, and evaporated to dryness to obtain the deprotected product. Full compound details are available in the [Supporting Information](#).

**General Procedure C: N-Alkylation.** The appropriate amine (1–10 g, 1.0 equiv) was dissolved in CH<sub>3</sub>CN (10–100 mL), followed by addition of 4-iodobenzyl bromide or 4-bromobenzyl bromide (1.1 equiv) and K<sub>2</sub>CO<sub>3</sub> (2.0 equiv) and the solution heated to reflux for 16 h. The solution was filtered, concentrated and the residue purified by column chromatography (silica gel, petroleum spirit/EtOAc, 50:50). Full compound details are available in the [Supporting Information](#).

**General Procedure D: Synthesis of Stannanes.** The desired brominated compound (10, 14, 21, 24, 42, 45, 48, 54) or literature iodinated 4 (~100 mg) was dissolved in toluene (~20 mL), and while under nitrogen atmosphere, hexamethylditin (1.1 equiv) and Pd-(PPh<sub>3</sub>)<sub>4</sub> (0.1 equiv) were added and the mixture was heated to 80 °C for 16 h. The reaction was monitored by TLC (either petroleum spirit/EtOAc solutions or EtOAc/CH<sub>3</sub>OH solutions). The reaction mixture was filtered over Celite and evaporated to dryness. The crude material was purified by silica gel chromatography (either petroleum spirit/EtOAc solutions or EtOAc/CH<sub>3</sub>OH solutions), followed by preparative HPLC. Full details for stannyl radiolabeling precursors (11, 15, 22, 25, 43, 46, 49, 55, and 56) are available in the [Supporting Information](#).

**Radiochemistry.** An ethanolic solution (100 μL of 1 mg/mL) of the stannyl precursor (11, 15, 22, 25, 43, 46, 49, and 55 and 56) was treated with a solution of Na<sup>123</sup>I (370–555 MBq) followed by chloramine-T (100 μL, 1 mg/mL H<sub>2</sub>O) and 1 M HCl (100 μL). After 5 min at room temperature (rt) the solution was quenched with Na<sub>2</sub>S<sub>2</sub>O<sub>5</sub> (100 μL, 50 mg/mL H<sub>2</sub>O) and neutralized with NaHCO<sub>3</sub> (100 μL, 50 mg/mL H<sub>2</sub>O). The crude reaction mixture was diluted with H<sub>2</sub>O (10 mL) and loaded onto an activated Waters Sep-Pak C18 Light cartridge (cartridges were activated with ethanol (2 mL) and then washed with water (15 mL) before use). The cartridge was eluted with CH<sub>3</sub>CN (~0.7 mL) and the eluate diluted with H<sub>2</sub>O (~0.7 mL) and purified on a semipreparative C18 RP HPLC column using conditions described in Table 1. HPLC purification was performed using a Waters Empower 2 system using a Waters 600 pump, Waters in-line degasser AF, Waters 2489 UV/visible detector measured at 254 nm, Carroll & Ramsey radioactivity detector, and a 7725i Rheodyne injector valve. The product was collected, diluted with H<sub>2</sub>O (10 mL), and loaded onto an activated Waters Sep-Pak C18 Light cartridge. The cartridge was eluted with EtOH (1 mL) and the solvent dried in vacuo and then formulated in saline solution with <5% ethanol for biological evaluation. In this formulation, tracers were found to be stable with purity of >95% up to 3 h.

**Animals.** Animal experiments were performed according to the Australian Code of Practice for the Care and Use of Animals for Scientific Purposes and were approved by the ANSTO Animal Care and Ethics Committee. Female C57BL/6J mice aged 5–6 weeks old were obtained from the Animal Resource Centre (Perth, Australia). The animals were kept at a constant temperature of 22 ± 2 °C on a 12–12 h light–dark cycle with light on at 09:00 a.m. Food and water were freely available.

**Cell Culture and Tumor Induction.** The B16F0 murine melanotic melanoma cells were originally obtained from the European Collection of Cell Cultures (ECACC, U.K.) and cultured in RPMI-1640 supplemented with 10% fetal calf serum at 37 °C under 5% CO<sub>2</sub>/95% atmosphere. Cells were grown to subconfluent monolayers

before being detached using trypsin for use in animal models. After a week of acclimatization, mice were subcutaneously inoculated on the left flank with  $3 \times 10^5$  B16F0 cells in 100  $\mu\text{L}$  of  $\text{Ca}^{2+}/\text{Mg}^{2+}$ -free phosphate buffered saline. The procedure was performed without anesthetic. B16F0 tumors were allowed to develop for 11 days before the animals were used in experimentation with  $\sim 77$ –100% of the animals having developed desirable-sized tumors. Tumors used in experiments were 2–12 mm in diameter.

**SPECT Imaging Studies.** The whole-body distribution of [ $^{123}\text{I}$ ]9, [ $^{123}\text{I}$ ]13, [ $^{123}\text{I}$ ]20, [ $^{123}\text{I}$ ]23, [ $^{123}\text{I}$ ]41, [ $^{123}\text{I}$ ]44, [ $^{123}\text{I}$ ]47, [ $^{123}\text{I}$ ]53, and [ $^{123}\text{I}$ ]4 in B16F0 tumor bearing C57BL/6J mice was followed over 72 h using SPECT imaging. The procedure was performed using a high-resolution  $\gamma$ -camera (X-SPECT; Gamma Medica Inc., USA) designed for laboratory animals and equipped with an array of discrete 2 mm  $\times$  2 mm  $\times$  6 mm NaI(Tl) crystals optically isolated from each other and a high-resolution, parallel-hole collimator of 12.5 cm  $\times$  12.5 cm field of view. Animals ( $n = 3$ , per tested compound) were injected with 18–20 MBq of radiotracer (in 100  $\mu\text{L}$  volume) through the lateral vein before being anesthetized via inhalant isoflurane (forthane, 5% induction, and 2–2.5% maintenance) in 200 mL/min oxygen delivered through a nose-cone fitted to the animal bed. Body temperature was maintained using a heating pad set at 37  $^\circ\text{C}$  and respiration rate monitored throughout the scanning period using a pressure sensor (BioVet, m2m Imaging Corp, USA). Mice were planar imaged at 10–60 min (5 min frames), 3 and 6 h (10 min), 24 h (20 min), 48 h (40 min), 72 h (60 min) (tumor permitting) and were recovered from anesthetic with access to food and water between scans.

SPECT images were analyzed by drawing a region of interest (ROI) around the tumor, and the lung as a background region which represents the mediastinal blood pool excluding regions of tracer accumulation. The lung ROI was chosen as background for maximum pixel value (MPV) calculation, as it results in a more conservative estimation for the differences in tumor to nontumor comparisons due to lower attenuation of the photon through the lung region which is predominantly air. The MPV within the ROI was then divided by the maximum pixel value within the background ROI to determine a tumor to nontumor ratio. Further to this, corrections were made to the MPV for radioactivity decay, including for scan length so that activity–time course kinetic information on the radiotracer for the regions could be determined.

**Biodistribution Studies.** [ $^{123}\text{I}$ ]20, [ $^{123}\text{I}$ ]23, [ $^{123}\text{I}$ ]41, and [ $^{123}\text{I}$ ]53 (0.37–1.85 MBq, 100  $\mu\text{L}$ ) were injected intravenously into C57BL/6J mice via the tail vein. Animals for time points of 1–24 h were injected with approximately 0.37 MBq of the radiotracers, and 1.85 MBq was injected for the 48 h time point. Postinjection points of 1, 3, 6, 16, 24, and 48 h were chosen for determining the distribution of compounds in tumors and in various organs and tissues. At the defined time point, mice were sacrificed, selected organs were dissected, weighed, and the radioactivity was measured with a Wallac 1480  $\gamma$ -counter (PerkinElmer, MA, USA). The fraction of injected activity [percent injected dose (% ID)] in the organ was calculated by comparison with suitable dilutions of the injected dose. Then, the radioactivity concentration in the organ (% ID/g) was ascertained by dividing the % ID for each organ by the weight of the organ, assuming a uniform density of 1 g/ $\text{cm}^3$ . After decay correction, data were normalized with the individual injected dose for each animal, the standard mouse body weighed (20 g), then corrected for the tail injected dose. The remaining activity in the carcass was also determined in order to obtain the total activity in the mouse at each time point.

Areas under the curves (AUCs) of the tumor and selected radiosensitive organs were calculated using GraphPad Prism, version 5.04 (CA, USA). Tumor-to-radiosensitive organ AUC ratios (AUCRs) were calculated by dividing the tumor AUC by a corresponding organ AUC. Data from Table 3 are presented as the mean of percentage of injected dose per gram of tissues (% ID/g)  $\pm$  SEM,  $n = 5$ , and as the mean of tumor-to-radiosensitive organ AUC ratios (AUCRs)  $\pm$  SEM,  $n = 5$ , which were derived from the biodistribution study.

Raw data were analyzed for significant outliers by Grubb tests, and none were detected. Statistical analyses were performed using GraphPad Prism, version 5.04 (CA, USA). Separate within one-way

ANOVA analyses (radiotracers as independent factor) followed by Bonferroni post hoc tests were employed to determine the level of statistically significant variation in the tumor-to-radiosensitive organ AUC ratios among the radiotracers. Significance was set at  $P \leq 0.05$ .

**Metabolite Studies.** The amounts of intact [ $^{123}\text{I}$ ]20, [ $^{123}\text{I}$ ]23, [ $^{123}\text{I}$ ]41, and [ $^{123}\text{I}$ ]53 in the tumor, eyes, spleen, urine, and plasma, of B16F0 tumor bearing C57BL/6J mice, were quantified by radio-HPLC and radio-TLC analysis at 3 and 24 h after injection of 20 MBq of the radiotracer. After the samples were initially collected, they were placed in a  $\gamma$  counter (PerkinElmer 1480 Wallace Wizard 3) and the activity (cpm) and time of measurement were recorded.

Whole organ tissue samples (tumor, eyes, and spleen) were suspended in  $\text{CH}_3\text{CN}/\text{water}$  (3:2, 500  $\mu\text{L}/50$  mg tissue), 5  $\mu\text{L}$  of the corresponding nonradioactive iodine standard (1 mg/mL in  $\text{CH}_3\text{OH}$ ) and 5  $\mu\text{L}$  KI (1 mg/mL in water) were added, and the sample was exposed to an ultrasonic probe (Ultrasonic Processor, Misonix Inc., Farmingdale, NY, USA) for 2 min before being centrifuged at 5000 rpm for 5 min. The supernatant was removed, and the radioactivity of the precipitate was measured using a  $\gamma$  counter to quantify the extraction efficiency. If necessary, a second extraction was performed to ensure maximum recovery of the radioactivity. An appropriate amount of the supernatant, based on the activity level (cpm), was collected ( $\sim 100$   $\mu\text{L}$ ) and diluted with water (up to 1.5 mL) for HPLC analysis or evaporated to dryness on a rotary evaporator under vacuum for TLC analysis.

To the urine (10  $\mu\text{L}$  diluted to 1 mL with water) were added 5  $\mu\text{L}$  of the corresponding nonradioactive iodine standard (1 mg/mL in  $\text{CH}_3\text{OH}$ ) and 5  $\mu\text{L}$  KI (1 mg/mL in water) before being analyzed by HPLC and TLC. For HPLC analysis, plasma (50  $\mu\text{L}$ ) was mixed with 5  $\mu\text{L}$  of the corresponding nonradioactive iodine standard (1 mg/mL in  $\text{CH}_3\text{OH}$ ) and 5  $\mu\text{L}$  KI (1 mg/mL in water) before being analyzed by HPLC. For TLC analysis, plasma (50  $\mu\text{L}$ ) was mixed with 5  $\mu\text{L}$  of the corresponding nonradioactive iodine standard (1 mg/mL in  $\text{CH}_3\text{OH}$ ), 5  $\mu\text{L}$  KI (1 mg/mL in water), and  $\text{CH}_3\text{CN}$  (500  $\mu\text{L}$ ) before being centrifuged (Heraeus Biofuge primoR centrifuge) at 5000 rpm for 5 min; the supernatant was analyzed by TLC.

The TLC samples were diluted with  $\text{CH}_3\text{OH}$  (25–50  $\mu\text{L}$ ) before being applied to the concentrating zone of the silica TLC plate in conjunction with the corresponding [ $^{123}\text{I}$ ] labeled and nonradioactive iodine standard. Varied TLC solvent systems of  $\text{EtOAc}/\text{CH}_3\text{OH}$  + aqueous ammonia solution (200 mL) were utilized for the four [ $^{123}\text{I}$ ]tracers analyzed: [ $^{123}\text{I}$ ]20 95:5 + 10 drops; [ $^{123}\text{I}$ ]23 90:10 + 10 drops; [ $^{123}\text{I}$ ]41 and [ $^{123}\text{I}$ ]53 85:15 + 10 drops. Visualizing the retention of the nonradioactive standard spots was by a UV lamp, while the radioactive spots were visualized using a phosphorimager (Typhoon FLA 7000 Phosphorimager, GE Healthcare, Rydalmere, Australia, with Fuji Film Multigage 3.0 software). The intact tracer was identified as the radioactive spot containing the identical  $R_f$  value corresponding to the nonradioactive standard observed under the UV lamp. Integration of the active spot in relation to all the activity in the TLC lane gave the percentage of intact tracer.

Radio-HPLC for metabolite analysis was performed using a Waters Empower 2 system using a two-stage pump system including a Waters 515 isocratic pump and a Waters 600 gradient pump, Waters in-line degasser AF, Waters 2489 UV/visible detector measured at 254 nm, IN/US Systems Posi-Ram detector, and a 7725i Rheodyne injector valve. The separation followed the method of Hilton et al.<sup>20</sup> A precolumn (Waters Oasis HLB, 25  $\mu\text{m}$ , 20 mm  $\times$  3.9 mm) and a reverse phase HPLC column (Phenomenex Bondclone C18, 10  $\mu\text{m}$ , 250 mm  $\times$  4.6 mm or Phenomenex Synergi Max-RP 80A C18, 4  $\mu\text{m}$ , 250 mm  $\times$  4.6 mm) in series, with a switching valve between columns, was utilized (Table 6). The precolumn was washed with 1%  $\text{CH}_3\text{CN}$  in water for 3 min at 1.5 mL/min, and then the solvent direction was switched to include the HPLC column. Both columns in series were then eluted over 10 min. The radioactivity peak corresponding to the nonradioactive standard was compared to the total activity registered in the radiochromatogram to give the fraction of unchanged ligand in the sample.

**Table 6. HPLC Chromatographic Conditions Used for Metabolite Studies**

analysis	column	chromatographic conditions (CH <sub>3</sub> CN/modifier, v:v)	flow rate (mL/min)
[ <sup>123</sup> I]20	Phenomenex Synergi	50:50 <sup>a</sup>	1.0
[ <sup>123</sup> I]23	Phenomenex Bondclone	60:40 <sup>b</sup>	1.5
[ <sup>123</sup> I]41	Phenomenex Bondclone	70:30 <sup>a</sup>	1.0
[ <sup>123</sup> I]53	Phenomenex Bondclone	50:50 <sup>b</sup>	1.5

<sup>a</sup>0.1 M NH<sub>4</sub>C<sub>2</sub>H<sub>3</sub>O<sub>2</sub>, <sup>b</sup>0.01 M NH<sub>4</sub>HCO<sub>3</sub>.

## ■ ASSOCIATED CONTENT

### 📄 Supporting Information

Full chemical characterization, extended NMR discussion, entire SPECT images, full biodistribution, metabolite data, and a csv file containing molecular formula strings. The Supporting Information is available free of charge on the ACS Publications website at DOI: 10.1021/acs.jmedchem.5b00777.

## ■ AUTHOR INFORMATION

### Corresponding Author

\*E-mail: Ivan.Greguric@ansto.gov.au. Phone: +(61) 2 9717 3759. Fax: +(61) 2 9717 9262.

### Present Addresses

<sup>||</sup>A.M.K.-H.: National Deuteration Facility, Australian Nuclear Science and Technology Organisation, NSW, Australia.

<sup>⊥</sup>S.R.T.: Department of Nuclear Medicine, Royal Brisbane and Women's Hospital, QLD, Australia.

<sup>#</sup>D.D.: Centre for Cellular and Molecular Biology, School of Life and Environmental Sciences, Deakin University, Burwood, Victoria, Australia.

<sup>∇</sup>A.K.: Department of PET & Nuclear Medicine, Royal Prince Alfred Hospital, NSW, Australia.

### Author Contributions

<sup>§</sup>M.P.R. and V.N. contributed equally.

### Notes

The authors declare no competing financial interest.

## ■ ACKNOWLEDGMENTS

We gratefully acknowledge the Cooperative Research Centre for Biomedical Imaging Development (CRCBID) for financial support. We thank Xiang Liu and Branko Dikic for chemical synthesis. We thank Kerynne Belbin, Geetanjali Dhand, and Emma Millard for assistance with animal studies and Iveta Kurlapski for chemical and radiochemical technical assistance.

## ■ ABBREVIATIONS USED

CH<sub>3</sub>CN, acetonitrile; AUC, areas under the curve; AUCR, ratio of areas under the curve; CH<sub>2</sub>Cl<sub>2</sub>, dichloromethane; dpm, disintegrations per minute; DIPEA, *N,N*-diisopropylethylamine; DMF, dimethylformamide; equiv, equivalent; EtOH, ethanol; EtOAc, ethyl acetate; EDC, 1-ethyl-3-(3-dimethylaminopropyl)carbodiimide; HPLC, high performance liquid chromatography; HR-MS, high-resolution mass spectrometry; h, hour; HOBT, hydroxybenzotriazole; NMR, nuclear magnetic resonance; % ID/g, percent of injected dose per gram; <sup>123</sup>I, iodine-123; <sup>131</sup>I, iodine-131; LR-MS, low-resolution mass spectrometry; RP, reverse phase; rt, room temperature; SPECT, single photon emission computed tomography;

Pd(PPh<sub>3</sub>)<sub>4</sub>, tetrakis(triphenylphosphine)palladium(0); TLC, thin layer chromatography; TFA, trifluoroacetic acid

## ■ REFERENCES

- (1) *Cancer in Australia 2010: An Overview*; Cancer Series No. 60; Australian Institute of Health and Welfare & Australasian Association of Cancer Registries: Canberra, Australia, 2010.
- (2) *Cancer in Victoria: Statistics and Trends 2010*; Victorian Cancer Registry; Cancer Council Victoria: Melbourne, Australia, 2011.
- (3) Garbe, C.; Eigentler, T. K. Diagnosis and treatment of cutaneous melanoma: state of the art 2006. *Melanoma Res.* **2007**, *17*, 117–127.
- (4) Klein, M.; Lotem, M.; Peretz, T.; Zwas, S. T.; Mizrahi, S.; Liberman, Y.; Chisin, R.; Schachter, J.; Ron, I. G.; Iosilevsky, G.; Kennedy, J. A.; Revskaya, E.; de Kater, A. W.; Banaga, E.; Klutzaritz, V.; Friedmann, N.; Galun, E.; DeNardo, G. L.; DeNardo, S. J.; Casadevall, A.; Dadachova, E.; Thornton, G. B. Safety and efficacy of <sup>188</sup>-rhenium-labeled antibody to melanin in patients with metastatic melanoma. *J. Skin Cancer* **2013**, *2013*, 828329.
- (5) Jandl, T.; Revskaya, E.; Jiang, Z.; Bryan, R. A.; Casadevall, E. Complement-dependent cytotoxicity of an antibody to melanin in radioimmunotherapy of metastatic melanoma. *Immunotherapy* **2013**, *5* (4), 357–364.
- (6) Coderre, J. A.; Packer, S.; Fairchild, R. G.; Greenberg, D.; Laster, B.; Micca, P.; Fand, I. Iodothiouracil as a melanoma localizing agent. *J. Nucl. Med.* **1986**, *27* (7), 1157–1164.
- (7) SeEVERS, R. H.; Counsell, R. E. Radioiodination techniques of small organic molecules. *Chem. Rev.* **1982**, *82*, 575–590.
- (8) Stocklin, G. Bromine-<sup>77</sup> and iodine-<sup>123</sup> radiopharmaceuticals. *Int. J. Appl. Radiat. Isot.* **1977**, *28*, 131–147.
- (9) Mani, R. S. *Radionuclides Production*; Leus, F., Ed.; CRC Press: Boca Raton, FL, 1983.
- (10) Chezal, J.; Papon, J.; Labarre, P.; Lartigue, C.; Galmier, M.; Decombat, C.; Chavignon, O.; Maublant, J.; Teulade, J.; Madelmont, J.; Moins, N. Evaluation of radiolabelled (hetero)aromatic analogues of *N*-(2-diethylaminoethyl)-4-iodobenzamide for imaging and targeted radionuclide therapy of melanoma. *J. Med. Chem.* **2008**, *51*, 3133–3144.
- (11) Sillaire-Houtmann, I.; Bonafous, J.; Veyre, A.; Mestas, D.; d'Incan, M.; Moins, N.; Kemeny, J.-L.; Chossat, F.; Bacin, F. Étude clinique en phase 2 de la BZA2 (<sup>123</sup>IN-(2-diéthylaminoéthyl)-2-iodobenzamide) dans le diagnostic du mélanome malin oculaire et de ses métastases. *J. Fr. Ophthalmol.* **2004**, *27*, 34–39.
- (12) Michelot, J. M.; Moreau, M. F. C.; Veyre, A. J.; Bonafous, J. F.; Bacin, F. J.; Madelmont, J. C.; Bussiere, F.; Souteyrand, P. A.; Mauclair, L. P.; Chossat, F. M.; Papon, J. M.; Labarre, P. G.; Kauffmann, P.; Plagne, R. J. Phase II scintigraphic clinical trial of malignant melanoma and metastases with iodine-123-N-(2-diethylaminoethyl 4-iodobenzamide). *J. Nucl. Med.* **1993**, *34* (8), 1260–1266.
- (13) Brandau, W.; Niehoff, T.; Pulawski, P.; Jonas, M.; Dutschka, K.; Sciuk, J.; Coenen, H. H.; Schober, O. Structure distribution relationship of iodine-123-iodobenzamides as tracers for the detection of melanotic melanoma. *J. Nucl. Med.* **1996**, *37* (11), 1865–1871.
- (14) Moins, N.; D'Incan, M.; Bonafous, J.; Bacin, F.; Labarre, P.; Moreau, M.-F.; Mestas, D.; Noirault, E.; Chossat, F.; Berthommier, E.; Papon, J.; Bayle, M.; Souteyrand, P.; Madelmont, J.-C.; Veyre, A. <sup>123</sup>I-N-(2-Diethylaminoethyl)-2-iodobenzamide: a potential imaging agent for cutaneous melanoma staging. *Eur. J. Nucl. Med. Mol. Imaging* **2002**, *29* (11), 1478–1484.
- (15) Dittmann, H.; Coenen, H. H.; Zolzer, F.; Dutschka, K.; Brandau, W.; Streffer, C. In vitro studies on the cellular uptake of melanoma imaging aminoalkyl-iodobenzamide derivatives (ABA). *Nucl. Med. Biol.* **1999**, *26*, 51–56.
- (16) Bacin, F.; Michelot, J. M.; Bonafous, J.; Veyre, A.; Moreau, M. F.; Kemeny, J. L.; Chossat, F.; Bekhechi, D. Clinical study of [<sup>123</sup>I] *N*-(2-diethylaminoethyl)-4-iodobenzamide in the diagnosis of primary and metastatic ocular melanoma. *Acta Ophthalmol. Scand.* **1998**, *76*, 56–61.

- (17) Larisch, R.; Schulte, K.-W.; Vosberg, H.; Ruzicka, T.; Muller-Gartner, H.-W. Differential accumulation of iodine-123-iodobenzamide in melanotic and amelanotic melanoma metastases in vivo. *J. Nucl. Med.* **1998**, *39*, 996–1001.
- (18) Liu, X.; Pham, T. Q.; Berghofer, P.; Chapman, J.; Greguric, I.; Mitchell, P.; Mattner, F.; Loc'h, C.; Katsifis, A. Synthesis and evaluation of novel radioiodinated nicotinamides for malignant melanoma. *Nucl. Med. Biol.* **2008**, *35* (7), 769–781.
- (19) Billaud, E. M. F.; Rbah-Vidal, L.; Vidal, A.; Besse, S.; Tarrit, S.; Askienazy, S.; Maisonial, A.; Moins, N.; Madelmont, J.-C.; Miot-Noirault, E.; Chezal, J.-M.; Auzeloux, P. Synthesis, radiofluorination, and in vivo evaluation of novel fluorinated and iodinated radiotracers for PET imaging and targeted radionuclide therapy of melanoma. *J. Med. Chem.* **2013**, *56*, 8455–8467.
- (20) Chehade, F.; De Labriolle-Vaylet, C.; Michelot, J.; Moins, N.; Moreau, M. F.; Hindie, E.; Papon, J.; Escaig, F.; Galle, P.; A, V. Distribution of I-BZA (N-2-diethylaminoethyl-4-iodobenzamide) in grafted melanoma and normal skin: A study by secondary ion mass spectroscopy. *Cell. Mol. Biol.* **2001**, *47*, 529–534.
- (21) Guerquin-Kern, J. L.; Hillion, F.; Madelmont, J. C.; Labarre, P.; Papon, J.; Croisy, A. Ultra-structural cell distribution of the melanoma marker iodobenzamide: improved potentiality of SIMS imaging in life sciences. *Biomed. Eng. Online* **2004**, *3*, 10.
- (22) Joyal, J. L.; Barrett, J. A.; Marquis, J. C.; Chen, J.; Hillier, S. M.; Maresca, K. P.; Boyd, M.; Gage, K.; Nimmagadda, S.; Kronauge, J. F.; Friebe, M.; Dinkelborg, L.; Stubbs, J. B.; Stabin, M. G.; Mairs, R.; Pomper, M. G.; Babich, J. W. Preclinical evaluation of an <sup>131</sup>I-labeled benzamide for targeted radiotherapy of metastatic melanoma. *Cancer Res.* **2010**, *70*, 4045–4053.
- (23) Maisonial, A.; Kuhnast, B.; Papon, J.; Boisgard, R.; Bayle, M.; Vidal, A.; Auzeloux, P.; Rbah, L.; Bonnet-Duquennoy, M.; Miot-Noirault, E.; Galmier, M.-J.; Borel, M.; Askienazy, S.; Dolle, F.; Tavitian, B.; Madelmont, J.-C.; Moins, N.; Chezal, J.-M. Single photon emission computed tomography/positron emission tomography imaging and targeted radionuclide therapy of melanoma: new multimodal fluorinated and iodinated radiotracers. *J. Med. Chem.* **2011**, *54*, 2745–2766.
- (24) Viallard, C.; Perrot, Y.; Boudhraa, Z.; Jouberton, E.; Miot-Noirault, E.; Bonnet, M.; Besse, S.; Mishellany, F.; Cayre, A.; Maigne, L.; Rbah-Vidal, L.; D'Incan, M.; Cachin, F.; Chezal, J. M.; Degoul, F. [<sup>123</sup>I]ICF01012 melanoma imaging and [<sup>131</sup>I]ICF01012 dosimetry allow adapted internal targeted radiotherapy in preclinical melanoma models. *Eur. J. Dermatol.* **2015**, *1* (25), 29–35.
- (25) Pham, T. Q.; Greguric, I.; Liu, X.; Berghofer, P.; Ballantyne, P.; Chapman, J.; Mattner, F.; Dikic, B.; Jackson, T.; Loc'h, C.; Katsifis, A. Synthesis and evaluation of novel radioiodinated benzamides for malignant melanoma. *J. Med. Chem.* **2007**, *50* (15), 3561–3572.
- (26) Daumar, P.; Wanger-Baumann, C. A.; Pillarsetty, N. K.; Fabrizio, L.; Carlin, S. D.; Andreev, O. A.; Reshetnyak, Y. K.; Lewis, J. S. Efficient <sup>18</sup>F-labeling of large 37-amino-acid pHLIP peptide analogues and their biological evaluation. *Bioconjugate Chem.* **2012**, *23*, 1557–1566.
- (27) Pham, T. Q.; Berghofer, P.; Liu, X.; Greguric, I.; Dikic, B.; Ballantyne, P.; Mattner, F.; Nguyen, V.; Loc'h, C.; Katsifis, A. Preparation and biologic evaluation of a novel radioiodinated benzylpiperazine, <sup>123</sup>I-MEL037, for malignant melanoma. *J. Nucl. Med.* **2007**, *48* (8), 1348–1356.
- (28) Denoyer, D.; Hicks, R. J. Preclinical evaluation of <sup>131</sup>I-MEL037, unpublished data (Centre for Molecular Imaging, Peter MacCallum Cancer Centre, Melbourne, Australia).
- (29) Williams, L. A.; Pinto, L. H.; Gherson, J. The retinal pigment epithelium of wild type (C57BL/6J +/+) and pearl mutant (C57BL/6J pe/pe) mice. *Invest. Ophthalmol. Visual Sci.* **1985**, *26* (5), 657–669.
- (30) van der Heijden, A.; van Dijk, J. E.; Lemmens, A. G.; Beynen, A. C. Spleen pigmentation in young C57BL mice is caused by accumulation of melanin. *Lab. Anim.* **1995**, *29* (4), 459–463.
- (31) Sundberg, J. P. Pigmented spleens in C57BL mice. *Lab. Anim.* **1991**, *25* (1), 85–86.
- (32) Sundberg, J. P. Splenic melanosis in black mice. *JAX Notes*; The Jackson Laboratory: Bar Harbor, ME, 1989; Issue 439.
- (33) Veninga, T. S.; Wieringa, R. A.; Morse, H. Pigmented spleens in C57BL mice. *Lab. Anim.* **1989**, *23* (1), 16–20.
- (34) Greguric, I.; Taylor, S. R.; Denoyer, D.; Ballantyne, P.; Berghofer, P.; Roselt, P.; Pham, T. Q.; Mattner, F.; Bourdier, T.; Neels, O. C.; Dorow, D. S.; Loc'h, C.; Hicks, R. J.; Katsifis, A. Discovery of [<sup>18</sup>F]N-(2-(diethylamino)ethyl)-6-fluoronicotinamide: a melanoma positron emission tomography imaging radiotracer with high tumor to body contrast ratio and rapid renal clearance. *J. Med. Chem.* **2009**, *52* (17), 5299–5302.
- (35) Denoyer, D.; Greguric, I.; Roselt, P.; Neels, O. C.; Aide, N.; Taylor, S. R.; Katsifis, A.; Dorow, D. S.; Hicks, R. J. High-contrast PET of melanoma using <sup>18</sup>F-MEL050, a selective probe for melanin with predominantly renal clearance. *J. Nucl. Med.* **2010**, *51*, 441–447.
- (36) Ware, R.; Kee, D.; McArthur, G.; Brglevska, S.; Callahan, J.; Katsifis, A.; Roselt, P.; Bourdier, T.; Hicks, R. J. First human study of N-(2-(diethylamino)ethyl)-6-[<sup>18</sup>F]fluoropyridine-3-carboxamide (MEL050). *J. Nucl. Med.* **2011**, *52*, 415.